

## Supporting Information

### Thermo-cross-linkable fullerene for long-term stability of photovoltaic devices

Nabankur Deb <sup>a</sup>, Raghunath R. Dasari <sup>b</sup>, Karttikay Moudgil <sup>b</sup>, Jeff L. Hernandez <sup>b</sup>, Seth R. Marder <sup>a,b,c</sup>, Yan Sun <sup>d</sup>,  
Alamgir Karim <sup>d</sup> and David G. Bucknall <sup>a,c,e\*</sup>

<sup>a</sup> School of Materials Science and Engineering, Georgia Institute of Technology, Atlanta, GA 30332, USA

<sup>b</sup> School of Chemistry and Biochemistry, Georgia Institute of Technology, Atlanta, GA 30332, USA

<sup>c</sup> COPE, Georgia Institute of Technology, Atlanta, GA 30332, USA

<sup>d</sup> Department of Polymer Engineering, University of Akron, Akron, OH 44325, USA

<sup>e</sup> current address: School of Engineering and Physical Sciences, Heriot-Watt University, Edinburgh, EH14 4AS, UK

Contents	Pages
1. Materials and General Methods	S2
2. Synthesis Details	S2
3. Materials Characterization	S5
4. UV-vis absorption spectra	S8-
5. Device characterization of P3HT systems	S10
6. Avrami Analysis	S11
7. GIWAXS analysis	S11
8. AFM analysis of P3HT systems	S12
9. Device characterization of PBT7 systems	S13

## 1. Materials and General Methods

**General:** All chemicals were purchased from commercial sources and used as received, unless stated otherwise. Column chromatography was carried out using silica gel (46-63  $\mu\text{m}$ , Sorbent) as the stationary phase, and thin-layer chromatography (TLC) was performed on precoated silica-gel plates (0.25 mm thick, 60F254, EMD, Germany) and visualised under UV light. The NMR spectra were measured on Varian Mercury 300 MHz and 400 MHz spectrometers. The chemical shift values were referenced with the solvent residual proton signal as internal standard. Mass spectra were measured on an Applied Biosystems 4700 Proteomics Analyzer using negative mode MALDI. Elemental analyses were carried out by Atlantic Microlabs using a LECO 932 CHNS elemental analyser. Electrochemical measurements were carried out under nitrogen in dry deoxygenated 0.1 M tetra-*n*-butylammonium hexafluorophosphate in dry  $\text{CH}_2\text{Cl}_2$  using a CH Instruments CHI620D Electrochemical Workstation CHI620D and a conventional three-electrode cell with a glassy carbon working electrode, platinum wire counter electrode, and an Ag wire coated with AgCl as the pseudo-reference electrode. Potentials were referenced to ferrocenium/ferrocene by using internal ferrocene. Cyclic voltammograms were recorded at a scan rate of  $50 \text{ mV s}^{-1}$ . High performance liquid chromatography (HPLC) traces of the PCBCB collected on a Shimadzu Class-VP series HPLC system equipped with a SCL-10A system controller, a SPD-10AV UV-Vis detector, a SPD-M10A diode array detector, and a Chromegabond WR C18  $5\mu\text{m}$ ,  $120\text{\AA}$ ,  $150 \times 4.6 \text{ mm}$  column. The mobile phase adapted for the measurements was a THF in MeOH solution (40:60 v/v).

## 2. Synthesis details

### Synthesis of PCBCB

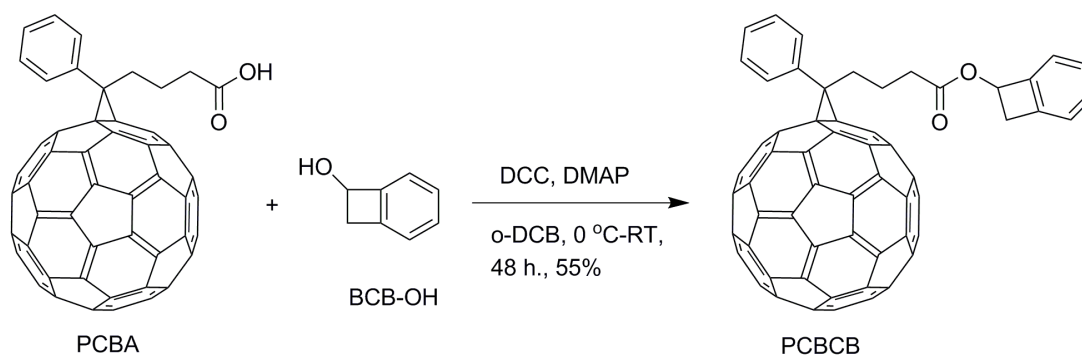


**Figure S1.** Synthesis of cross-linkable fullerene PCBCB.

PCBA (0.08 g, 0.09 mmol), 1-hydroxy benzocyclobutene (0.015 g, 0.13 mmol) and 4-dimethylaminopyridine (0.011 g, 0.09 mmol) was degassed in a flask and then dissolved in 45 mL of dichlorobenzene. The solution was sonicated for a

30 min to allow complete dissolution and then cooled to 0 °C (in an ice bath) and stirred for 5 min. *N,N'*-dicyclohexylcarbodiimide, DCC, (0.027 g, 0.13 mmol) was added to the solution and the mixture was stirred in ice bath for 3 hours before warming it to room temperature. It was then allowed to stir at room temperature for 48 h. The crude product collected was purified through column chromatography (silica, 50:50 v/v CH<sub>2</sub>Cl<sub>2</sub>/hexanes) to yield PCBCB (0.049 g, 55%). <sup>1</sup>H NMR (CD<sub>2</sub>Cl<sub>2</sub>, 300 MHz) δ 7.97-7.94 (m, 2H), 7.58-7.44 (m, 3H), 7.34-7.19 (m, 3H), 7.14 (d, *J* = 7.2 Hz, 1H), 5.88 (dd, *J* = 4.5, 2.1 Hz, 1H), 3.62 (dd, *J* = 14.4, 4.5 Hz, 1H), 3.19 (dm, *J* = 14.2, 1H), 2.97-2.91 (m, 2H), 2.57 (t, *J* = 7.2 Hz, 2H), 2.49-2.14 (m, 2H). <sup>13</sup>C(<sup>1</sup>H) NMR (CD<sub>2</sub>Cl<sub>2</sub>, 75 MHz) δ 173.2, 149.4, 149.3, 148.2, 146.3, 145.6, 145.5, 145.4, 145.3, 145.2, 145.1, 145.0, 144.9, 144.8, 144.7, 144.6, 144.3, 144.1, 143.4, 143.3, 143.3, 143.2, 143.2, 143.1, 142.6, 142.4, 141.2, 141.0, 138.4, 137.7, 137.2, 132.5, 130.3, 128.7, 128.5, 127.8, 123.8, 123.6, 80.4, 80.3, 71.9, 52.3, 39.2, 34.2, 33.9, 22.6. HRMS (MALDI) calculated for C<sub>79</sub>H<sub>18</sub>O<sub>2</sub> (M<sup>+</sup>), 998.1307; found 998.1304. Analysis calculated for C<sub>79</sub>H<sub>18</sub>O<sub>2</sub>: C, 94.98; H, 1.82. Found: C, 93.97; H, 1.72 (trace of CH<sub>2</sub>Cl<sub>2</sub> present in this sample, <sup>1</sup>H NMR of this sample in CDCl<sub>3</sub> showed the presence of trace amounts of CH<sub>2</sub>Cl<sub>2</sub> solvent).

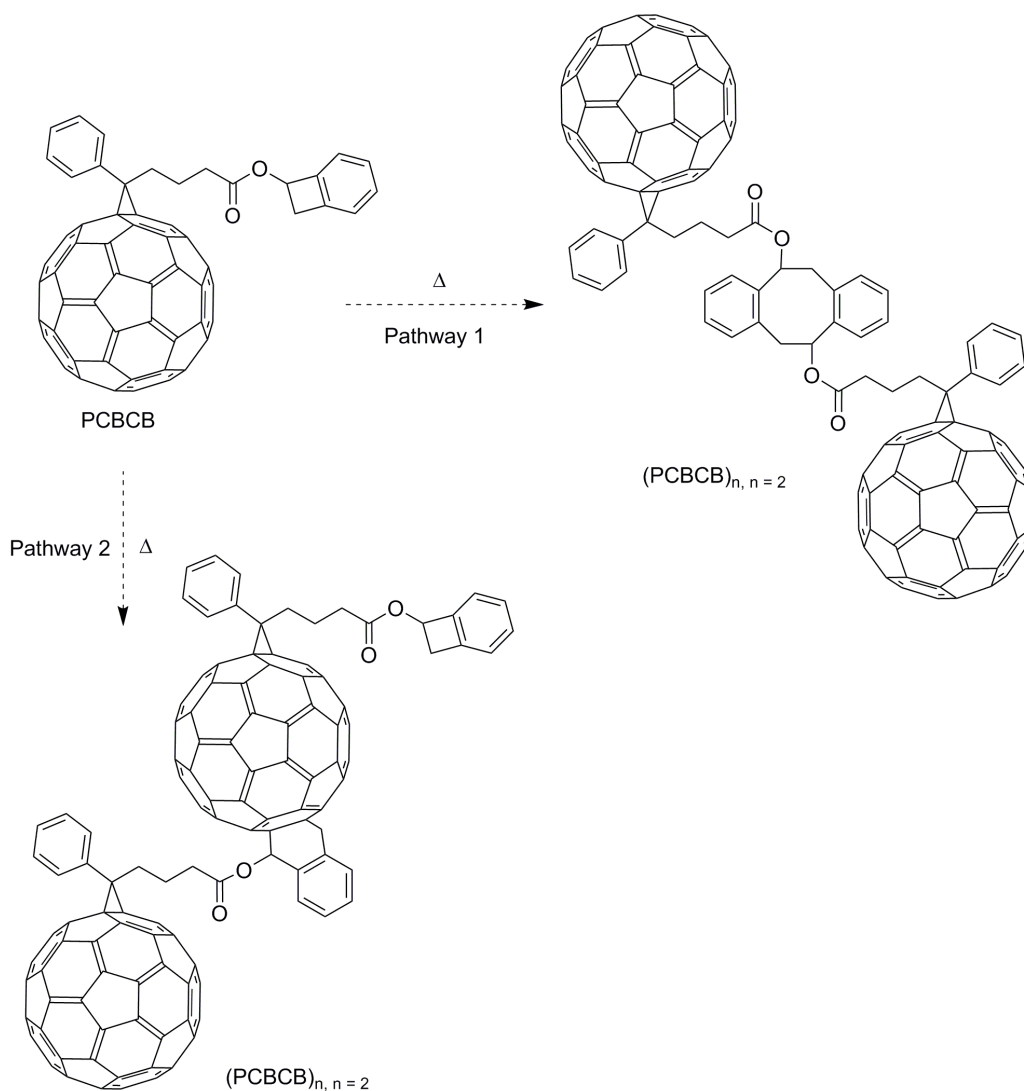


**Figure S2.** Schematic representation of oligomeric fullerene formation ((PCBCB)<sub>n</sub>, n = 2) via thermal cross-linking of PCBCB.

We anticipate thermal crosslinking of PCBCB occur through two pathways. One is based on the formation of quinodimethane intermediate and subsequently coupling to yield fullerene dimer.<sup>1</sup> Also, cycloaddition of quinodimethane intermediate with fullerenes has been observed in the literature as shown in pathway 2.<sup>2</sup>

## 3. Materials Characterization

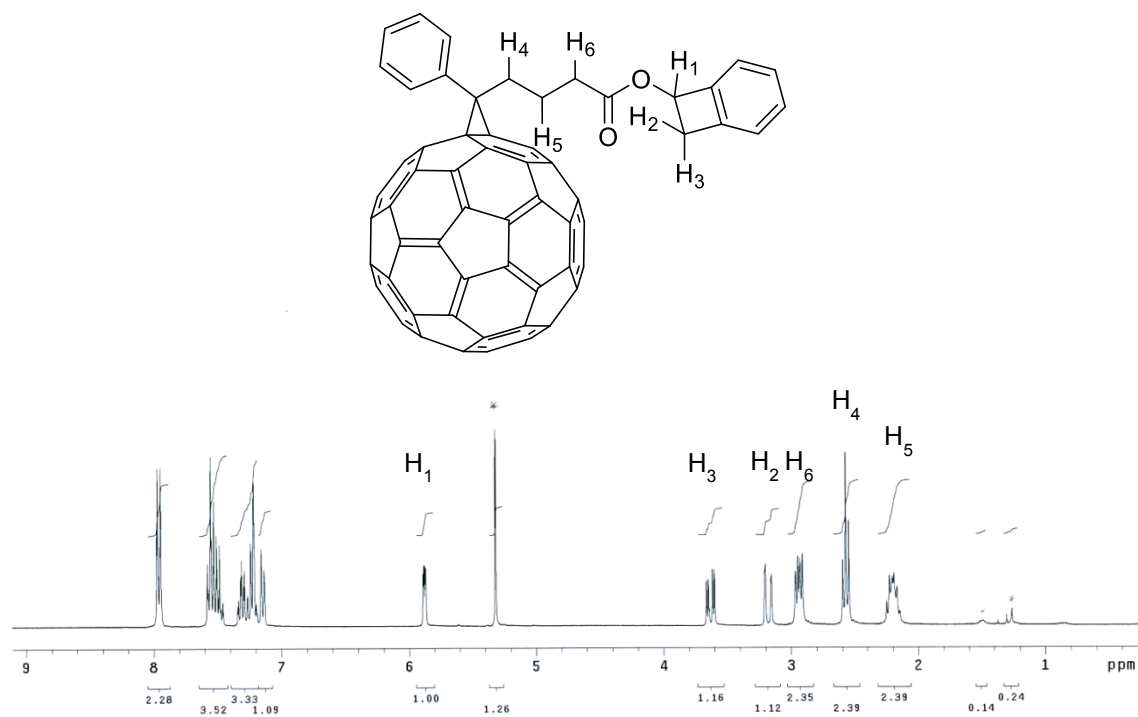


Figure S3.  $^1\text{H}$  NMR spectrum of PCBCB in CD<sub>2</sub>Cl<sub>2</sub>.

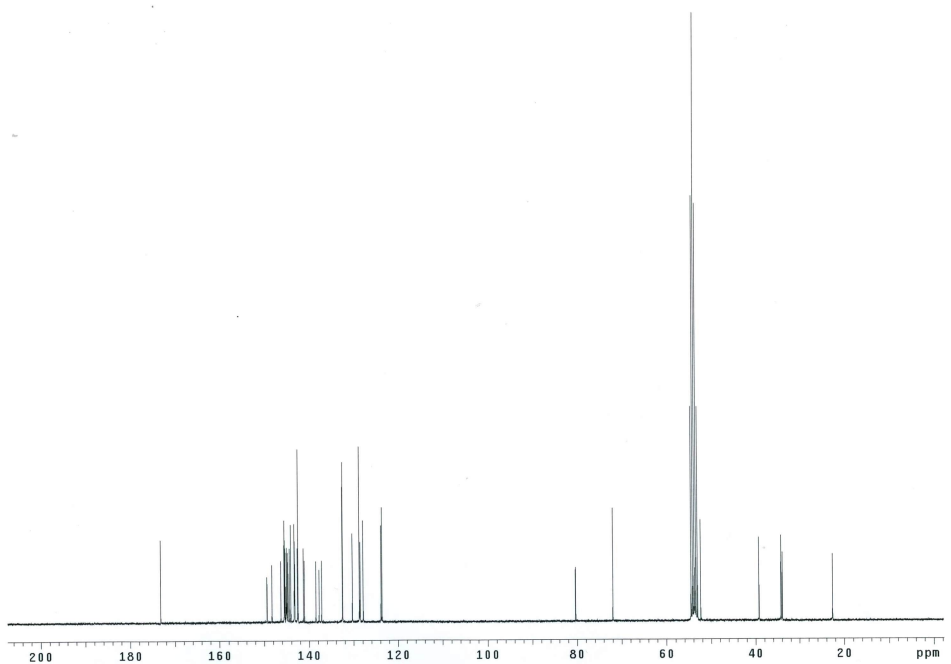
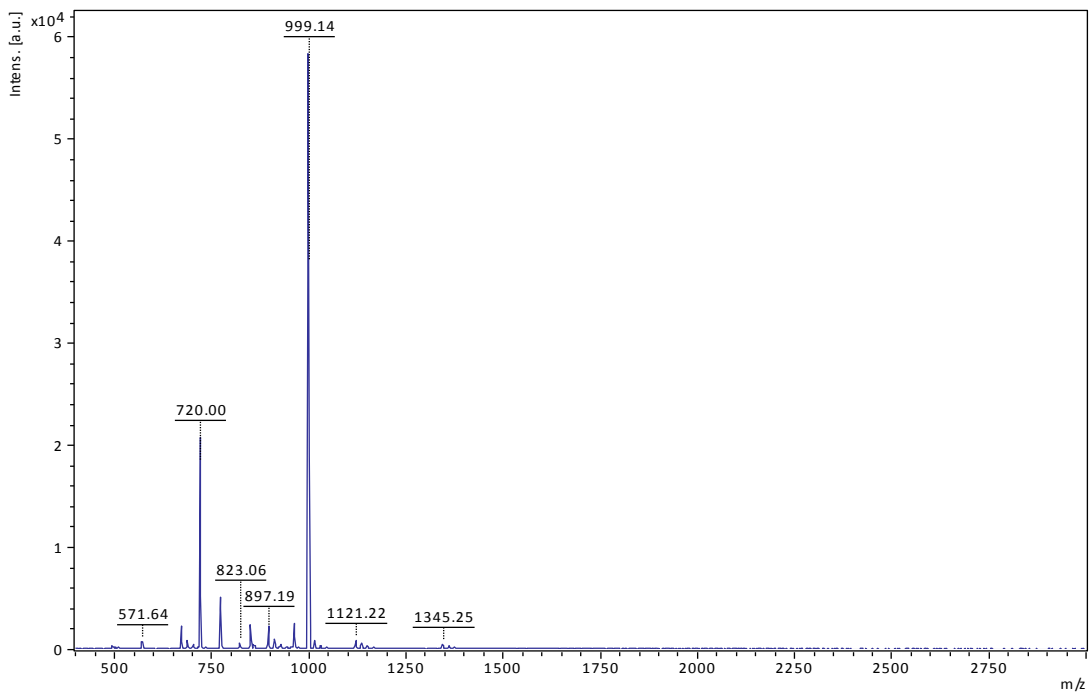
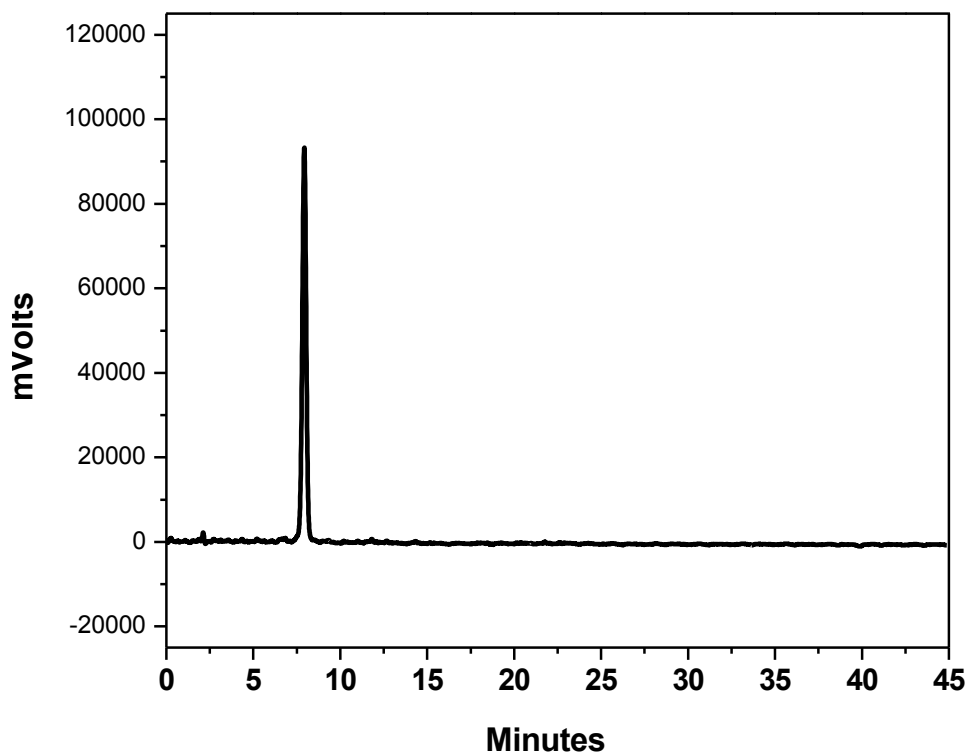


Figure S4.  $^{13}\text{C}$  NMR spectrum of PCBCB in CD<sub>2</sub>Cl<sub>2</sub>.



**Figure S5.** MALDI spectrum of PCBCB showing molecular ion peak (m/z 999).



**Figure S6.** HPLC trace of PCBCB in THF/MeOH (40:60 v/v) showing pure sample.

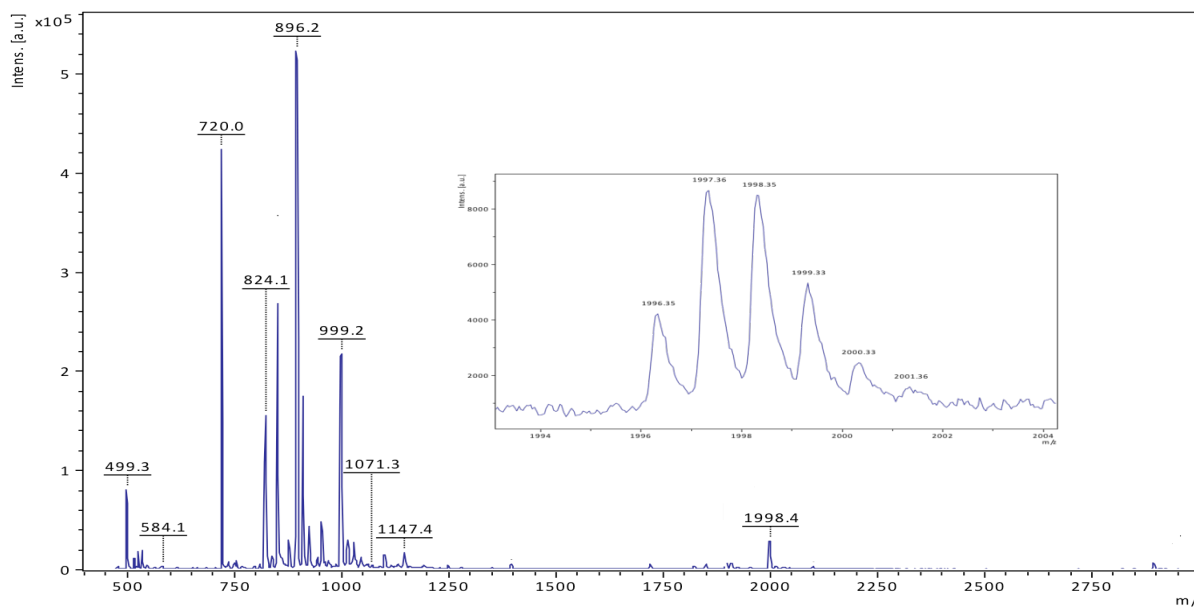


**Figure S7.** MALDI spectrum of (PCBCB) $_n$  where  $n = 2$ , showing the fullerene dimer ( $m/z$  1998) (Inset: showing isotope peaks of dimer molecular ion).

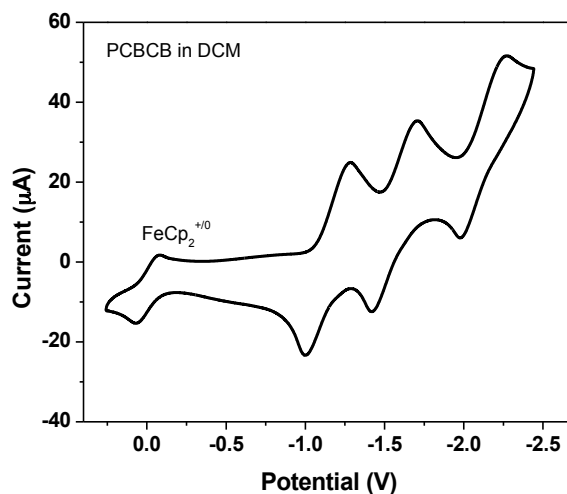


**Figure S8.** Cyclic voltammogram of PCBCB in  $\text{CH}_2\text{Cl}_2$ .

**Table S1.** Electrochemical<sup>a</sup> data of fullerenes

Material	$E_{1/2}^{(0/-)}/\text{V}$	$E_{1/2}^{(-2-)/\text{V}}$	$EA^b/\text{eV}$
PCBCB	-1.14	-1.56	3.66
PCBM	-1.11	-1.49	3.69

<sup>a</sup> 0.1 M  $n\text{Bu}_4\text{NPF}_6/\text{CH}_2\text{Cl}_2$  in V vs  $\text{FeCp}_2^{+/0}$ ; <sup>b</sup> Solid-state electron-affinity (EA) values estimated from  $EA = -eE_{1/2}^{(0/-)} + 4.8$  eV.

#### 4. UV-Vis absorption spectra

To determine the degree of crosslinking of the PCBCB precursor on annealing, UV-Vis spectra analysis was used. A calibration plot of the precursor was first determined using absorption measurements of solutions of different concentration (0.02, 0.01, 0.001 mg/ml) in  $\text{CH}_2\text{Cl}_2$  (Fig 5 a). Subsequently, drop cast films from the PCBCB precursor (1mg) in  $\text{CH}_2\text{Cl}_2$  (1 ml) were deposited on glass substrates and annealed for varying amounts of time. The films were subsequently washed with 1 ml of  $\text{CH}_2\text{Cl}_2$  each and sonicated to dissolve the non-crosslinked part of the film. These 1 ml solutions were twice diluted to 10 times their volume to bring the concentration within the range of the calibration value. The absorption spectra for those were then obtained (Fig 5b) and the intensity of the characteristic peak at  $\lambda_{\text{max}} = 330$  nm was obtained. The calibration plot was then used to determine the remaining concentration of the precursor in the annealed films (by measuring the intensity of the characteristic peaks in the solutions). This in turn determined the percentage conversion into the cross-linked product  $(\text{PCBCB})_n$  (Fig 5 c, Table 1). Annealing at 120 °C for 10 minutes (not shown here), all of the film was washed off leaving behind no insoluble cross-linked product. On the other end though, it could be seen that beyond annealing at 190 °C for 10 min, the percentage conversion increased minimally, suggesting that possibly the full conversion had taken place. The amount of conversion however was still not exactly 100%, which could possibly have arisen due to the fact that the film was not smooth and continuous everywhere, leading to areas where it was impossible for the precursor to encounter another molecule, and thus leaving behind some unreacted precursor. In addition, by varying the annealing temperature we saw the percentage conversion to the cross-linked fullerene could be varied, giving us a mechanism to control the degree of cross-linking in the fullerene. The increase isn't linear with temperature either so further studies can be carried out to fine-tune the thermal processing control of cross-linking.

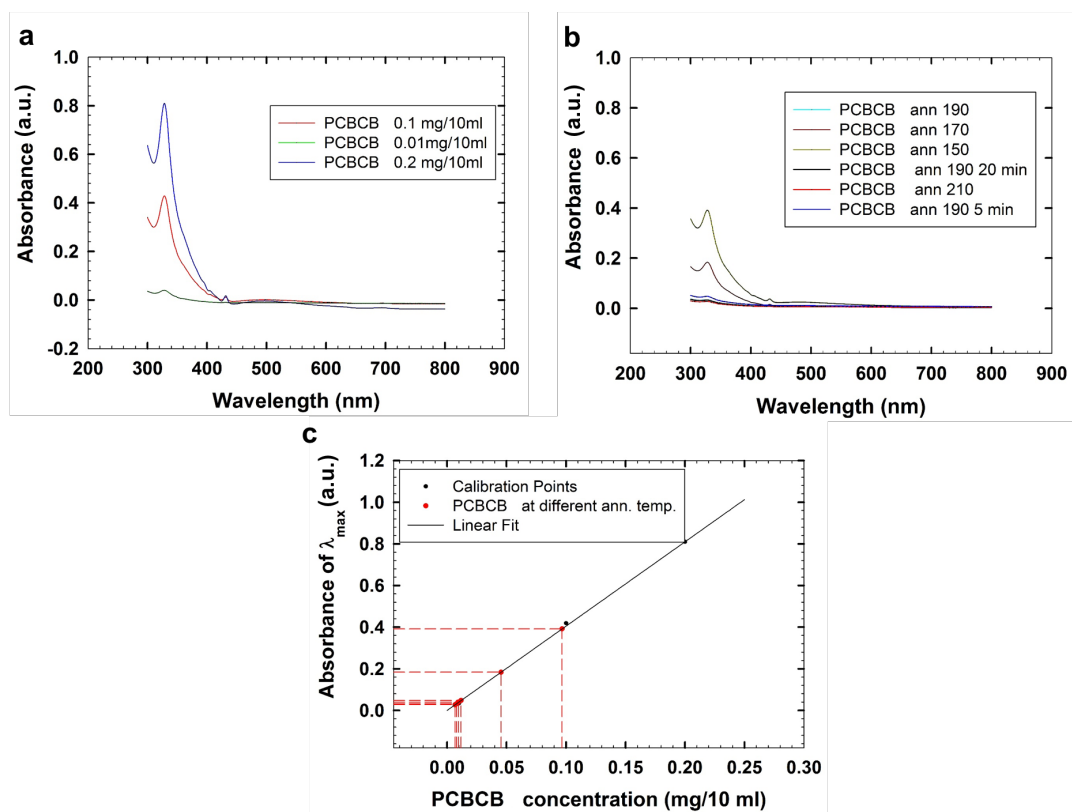


**Figure S9.** Absorption spectra of a) varying concentrations of PCBCB in  $\text{CH}_2\text{Cl}_2$  b) residual precursor from annealed samples of PCBCB at different temperatures (time =10 min unless otherwise mentioned) c) Calculation of percentage cross-link conversion of PCBCB to  $(\text{PCBCB})_n$  using a calibration plot

**Table S2.** Percentage conversion of PCBCB at different annealing temperatures

Sample	Conversion (%)
Annealed 150 °C	52.69
Annealed 170 °C	95.46
Annealed 190 °C	99.11
Annealed 210 °C	99.33
Annealed 190 °C 5 min	98.83
Annealed 190 °C 20 min	99.21

### 5. Device Characterization of P3HT-fullerene BHJs

SCLC data ( $J$  vs  $V$ ) was collected using devices made as was reported previously in literature.<sup>3</sup> The voltage is corrected for built-in voltage ( $V_{bi}$ ). A value of  $V_{bi} = 1.4$  eV was used and then the data was fitted to the equation (using Origin pro):

$$J = \frac{9}{8} \epsilon_0 \epsilon_r \mu_e \frac{V^2}{L^3} \quad [S1]$$

where  $J$  is the current,  $L$  is the layer thickness,  $V$  is the voltage,  $\epsilon_0$  and  $\epsilon_r$  are the permittivity of vacuum and the fullerene, respectively, and  $\mu_e$  is the electron mobility.

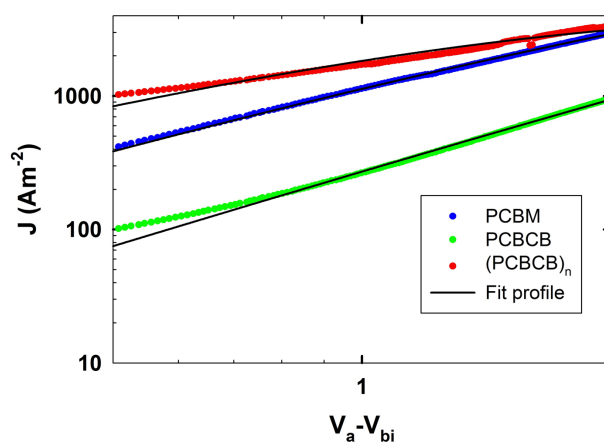


Figure S10. Electron mobility (SCLC) measurements and fits for PCBM, PCBCB and  $(PCBCB)_n$ .

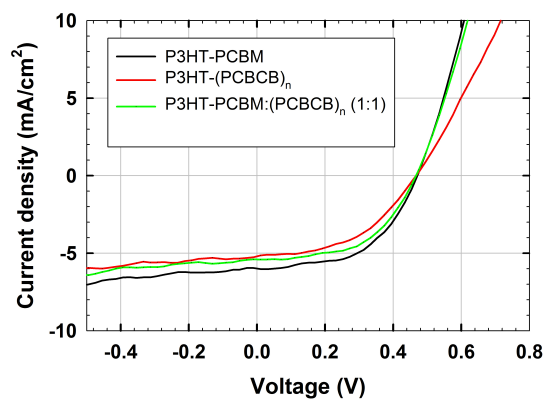


Figure S11. Initial current voltage statistics for BHJ devices built from different P3HT-fullerene mixtures.

**Table S3** Device efficiency parameters for BHJ devices built from different P3HT-Fullerene mixtures

Material	$J_{SC}$ (mA/cm <sup>2</sup> )	$V_{OC}$ (V)	$P_{MAX}$ (mW)	FF (%)	$\eta$ (%)
PCBM	5.99	0.47	0.10	51.71	1.47
(PCBCB) <sub>n</sub>	5.41	0.47	0.08	45.83	1.18
PCBM:(PCBCB) <sub>n</sub> (1:1)	5.41	0.47	0.09	51.68	1.33

## 6. Avrami Analysis

The Avrami equation in its simplest form can be used to determine the kinetics of PCBM crystallization.<sup>4</sup> It can be defined as:

$$\alpha(t) = 1 - \exp[-(kt)^n] \quad [S2]$$

In this  $\alpha(t)$  is the volume (or in our case area of the crystal at time  $t$ ),  $k$  is the rate constant and  $n$  is the Avrami exponent. By measuring the change in crystal dimension over a period of time (minimum 3 data points), the data can be fitted to the curve mentioned in equation S2 to give us the two variables,  $k$  and  $n$  (Fig S9).

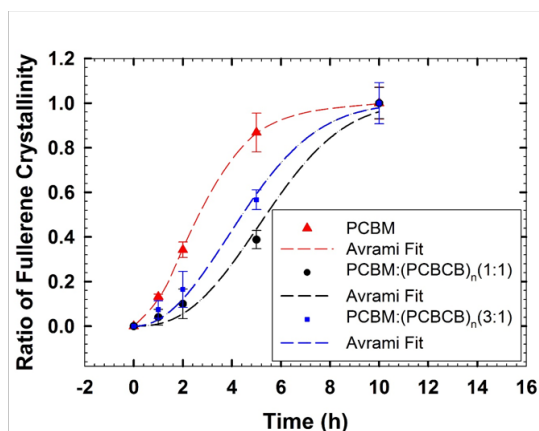


**Figure S12.** Avrami Fits for fullerene crystallization rates in BHJs.

## 7. GIWAXS analysis

2-D GIWAXS patterns and subsequent integration plots of PCBCB and (PCBCB)<sub>n</sub> showed an increase in the crystalline behavior upon formation of the cross-linked fullerene from the precursor, with the peak widths becoming visibly narrower (Fig S10, Table S3). Peak fitting consequently also gave us the value of the spacing between the fullerene groups, which for the cross-linked system was reduced, but minimally so. This suggested that even though the

crystallinity increases slightly upon cross-linking, it isn't large enough to decisively effect the increase in mobility that we observe. It may be one of several other reasons for the increase.

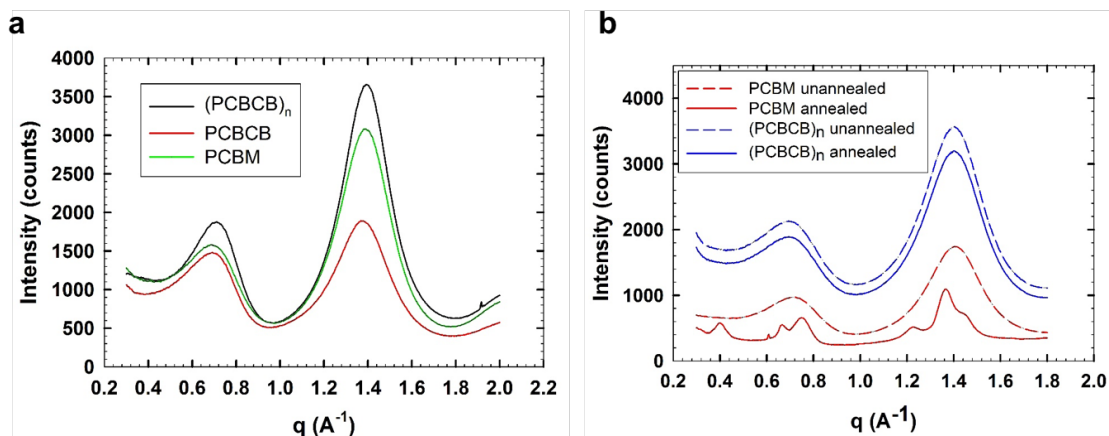


Figure S12. GIWAXS 1-d integration plots (I vs  $q$ ) for a) the fullerenes PCBM, PCBCB,  $(\text{PCBCB})_n$  b) comparison of PCBM and  $(\text{PCBCB})_n$  before and after annealing for 1 h at  $150^\circ\text{C}$

Table S4. Full width half max values and d-spacing for the characteristic peaks from GIWAXS analysis

Sample	FWHM( $\text{\AA}^{-1}$ )	d-spacing ( $\text{\AA}$ )
PCBM	0.36	4.56
PCBCB	0.28	4.52
$(\text{PCBCB})_n$	0.27	4.51
$(\text{PCBCB})_n$ annealed	0.27	4.51

## 8. AFM Analysis of P3HT-fullerene films

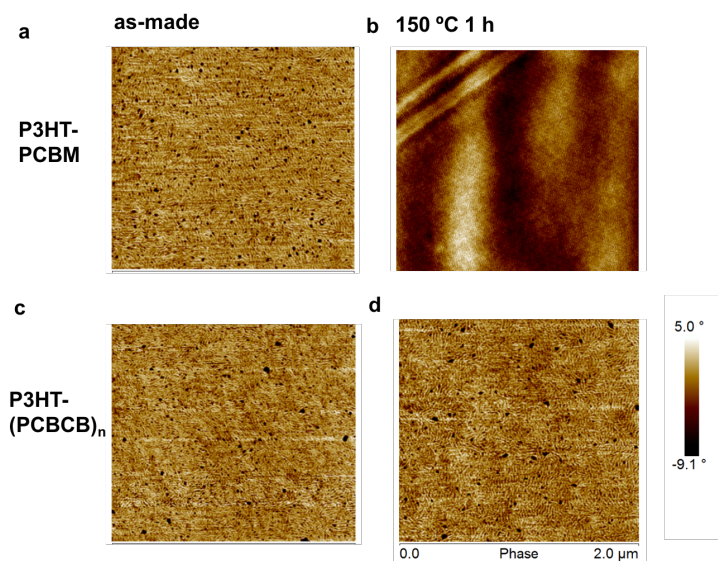
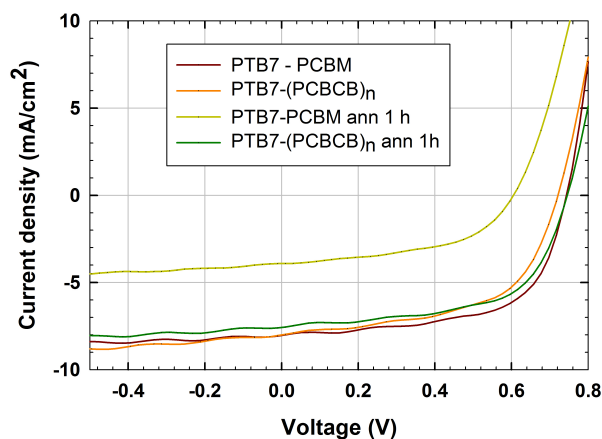


Figure S13. AFM phase images for a-b) P3HT-PCBM and c-d) P3HT- $(\text{PCBCB})_n$  based BHJs showing presence of nano-scale fullerene aggregates (dark spots) and b) formation of large scale fullerene aggregate on aging for 1 h at  $150^\circ\text{C}$

## 8 Device Characterization of PBT7-fullerene BHJs



**Figure S14.** Current voltage statistics for BHJ devices built from different PTB7-fullerene mixtures before and after 1h of accelerated aging/annealing at 150 °C

**Table S5.** Device efficiency parameters for BHJ devices built from different PTB7-Fullerene mixtures before and after 1 hour of annealing

Material	$J_{SC}$ (mA/cm <sup>2</sup> )	$V_{OC}$ (V)	$P_{MAX}$ (mW)	FF (%)	$\eta$ (%)
PTB7-PCBM	8.00	0.74	0.26	62.68	3.70
PTB7-(PCBCB) <sub>n</sub>	7.97	0.72	0.23	57.11	3.26
PTB7-PCBM 1h ann	3.91	0.62	0.09	50.70	1.22
PTB7-(PCBCB) <sub>n</sub> 1h ann	7.56	0.74	0.24	59.25	3.29

1. J. N. Dobish, S. K. Hamilton and E. Harth, *Polymer Chemistry*, 2012, **3**, 857-860.
2. A. Gügel, P. Belik, M. Walter, A. Kraus, E. Harth, M. Wagner, J. Spickermann and K. Müllen, *Tetrahedron*, 1996, **52**, 5007-5014.
3. V. D. Mihailetschi, J. K. J. van Duren, P. W. M. Blom, J. C. Hummelen, R. A. J. Janssen, J. M. Kroon, M. T. Rispens, W. J. H. Verhees and M. M. Wienk, *Advanced Functional Materials*, 2003, **13**, 43-46.
4. W.-R. Wu, U. S. Jeng, C.-J. Su, K.-H. Wei, M.-S. Su, M.-Y. Chiu, C.-Y. Chen, W.-B. Su, C.-H. Su and A.-C. Su, *ACS Nano*, 2011, **5**, 6233-6243.